MULTISCALE MODELLING OF CONCRETE PLATES USING THE BOUNDARY ELEMENT METHOD

CALEB G. PITALUGA & GABRIELA R. FERNANDES
Civil Engineering Department, Federal University of Catalão (UFCAT), Brazil

ABSTRACT

In this paper we analyse a concrete plate by using a multi-scale modelling technique. The boundary element nonlinear formulation for the two-dimensional problem is used to model the macrocontinuum while the concrete microstructure is modelled by a boundary element nonlinear formulation based on the concept of representative volume element (RVE) and considering it as a zoned plate where each sub-region represents a RVE phase. In both formulations the consistent tangent operator is used to achieve the convergence of the iterative procedures. The equilibrium problem of the plate is solved in terms of in-plane strains while for the RVE equilibrium problem it is done in terms of displacement fluctuations. To model the concrete microstructure, the Mohr–Coulomb criterion is used to govern the mechanical behaviour of the mortar matrix, while the aggregates are considered elastics. Besides, some voids are also defined in the mortar matrix to model the concrete porosity and the fracture process along the interfaces between matrix and aggregates are modelled by defining addition cohesive-contact finite elements superposed to the interface elements. To validate the presented model, the numerical results are compared to experimental ones.

Keywords: multi-scale modelling, homogenisation, RVE, boundary elements, 2D problem.

1 INTRODUCTION

In the present model, the concrete microstructure is numerically modelled by the representative volume element (RVE) formulation, and the RVE homogenised response defines the concrete constitutive model. For that, the strain tensor related to the macrocontinuum point must be imposed to the RVE and its equilibrium problem solved (see [1]–[6]). Therefore, to solve the multiscale problem of the plate, we must assign a RVE for each point considered in the plate equilibrium equation. Thus, in the present model two different formulations must be coupled to obtain the solution, both developed with the boundary element method (BEM): the formulation of the macrocontinuum (plate) (see Fernandes and de Souza Neto [7]) and the RVE formulation (concrete microstructure). As we deal with dissipative phenomena in the microstructure, both formulations require an iterative procedure to achieve the equilibrium of its respective problem. Thus, for each iteration of the macrocontinuum problem, we must solve an iterative procedure at each macrocontinuum point, where the RVE is assigned. Therefore, the multi-scale modelling is very expensive computationally, what encourages us to investigate other numerical models that reduce this computational effort, as the ones developed by the BEM.

In this study, to model the concrete microstructure, we consider the aggregates as elastic inclusions defined inside a mortar matrix, where some voids are also defined to model the concrete porosity. The Mohr–Coulomb criterion is adopted to govern the mechanical behaviour of the mortar (see Silva et al. [8]) and we define additional cohesive-contact finite elements on some interfaces to model the phase debonding phenomenon (see Pituba et al. [9]). These finite elements are defined superposed to BEM interface elements, being their mechanical behaviour governed by either a contact model or cohesive fracture model.

In the numerical example of a concrete plate subjected to compression load, we show that the present model can reproduce the experimental results (obtained in Delalibera [10]), showing its efficiency and accuracy.

WIT Transactions on Engineering Sciences, Vol 136, © 2024 WIT Press
www.witpress.com, ISSN 1743-3533 (on-line)
doi:10.2495/BE470121

2 MACRO-SCALE: THE NON-LINEAR TWO-DIMENSIONAL PROBLEM

Let us consider a plate of thickness *t*, represented by its middle surface defined in the plane (x_1, x_2), where the following values are defined in terms of normal and tangential directions: in-plane tractions ($\dot{p}_n$ and $\dot{p}_s$) and in-plane displacements ($\dot{u}_n$ and $\dot{u}_s$). As we deal with plasticity and fracture process at the material microstructure, all variables are expressed in their time derivatives, i.e., $(\dot{x}) = dx/dt$ or in terms of their increments (Δx). In this context, the total strain is split into its elastic ($\dot{\varepsilon}^e_{ij}$) and inelastic ($\dot{\varepsilon}^0_{ij}$) parts and the inelastic membrane force rate $\dot{N}^0_{ij}$, is defined as:

$$\dot{N}^0_{ij} = \dot{N}^e_{ij} - \dot{N}_{ij} \qquad i, j = 1, 2, \tag{1}$$

where the forces $\dot{N}_{ij}$ satisfy the constitutive model, and the forces $\dot{N}^e_{ij}$ are defined using the total strain $\dot{\varepsilon}_{ij}$ and the Hooke's law. For plane stress condition, they are given by:

$$\dot{N}^e_{ij} = \frac{\overline{E}}{(1-\nu^2)}\left[\nu \;\; \dot{\varepsilon}_{kk}\delta_{ij} + (1-\nu \;\;)\dot{\varepsilon}_{ij}\right] \qquad i, j, k = 1, 2, \tag{2}$$

where δ_{ij} is the Kronecker delta, $\bar{E} = Et$ being E the Young's modulus, ν the Poisson's ration. The integral representation for in-plane displacements can be obtained by applying the Betti's reciprocal theorem written in terms of forces $\dot{N}^e_{ij}$. After integrating by parts and considering eqn (1), we obtain the following representation of in-plane displacements:

$$K_i(q)\dot{u}_i(q) = -\int_\Gamma(\dot{u}_n p^*_{in} + \dot{u}_s p^*_{is})d\Gamma + \int_\Gamma(u^*_{in}\dot{p}_n + u^*_{is}\dot{p}_s)d\Gamma + \int_{\Omega_b}\left(u^*_{in}\dot{b}_n + u^*_{is}\dot{b}_s\right)d\Omega$$
$$+ \int_\Omega \varepsilon^*_{ijk}\dot{N}^0_{jk}\, d\Omega \qquad k, i, j = 1,2, \tag{3}$$

where q is the source point, the superscript * denotes the fundamental values; i denotes the fundamental load direction; Ω_b is the plate loaded area; the free term $K_i(q)$ is defined as $K_i(q) = 1$ and $K_i(q) = 1/2$, respectively, for internal and boundary points not coincident to corners. The integral representation for rotations is obtained by differentiating eqn (3):

$$\Delta u_{i,\ell}(q) = -\int_\Gamma(\Delta u_n p^*_{in,\ell} + \Delta u_s p^*_{is,\ell})d\Gamma + \int_\Gamma(u^*_{in,\ell}\,\Delta p_n + u^*_{is,\ell}\,\Delta p_s)d\Gamma$$
$$+ \int_{\Omega_b}(u^*_{in,\ell}\,\Delta b_n + u^*_{is,\ell}\,\Delta b_s)d\Omega + \int_\Omega \frac{\partial \varepsilon^*_{ijk}}{\partial x_l}\Delta N^0_{jk}\, d\Omega$$
$$+ \frac{1}{16\overline{G}(1-\nu')}\left[(6-8\nu')\dot{N}^0_{il}(q) - \dot{N}^0_{kk}(q)\delta_{il}\right] \qquad k, j, l = 1,2. \tag{4}$$

Now we must transform the integral representations (eqns (3) and (4)) into algebraic equations. For that, we consider linear elements where the displacements and tractions are approximated by quadratic functions. The elements are not discontinuous, i.e., their initial and final nodes correspond to the element extremities. At corners we adopt duplicate nodes and to write the algebraic equation for these nodes we move the node inside the element. Besides, we have also to discretise the plate domain because of the inelastic forces defined in the domain. For that we adopt triangular cells where the inelastic forces are approximated by linear functions. To write the set of equations necessary to obtain the boundary values, we consider the two in-plane displacements equation written in each boundary node. After

applying the boundary conditions to the boundary nodes, the unknown's vector on the plate boundary ($\Delta \boldsymbol{X}$) are computed from the following set of equations:

$$\Delta \boldsymbol{X} = \Delta \boldsymbol{L} + \boldsymbol{R}_N \Delta \boldsymbol{N}^0, \tag{5}$$

where vector $\Delta \boldsymbol{L}$ defines the elastic solution and $\boldsymbol{R}_N$ are the corrections due to the dissipative forces ($\Delta \boldsymbol{N}^0$).

In eqn (5) $\boldsymbol{R}_N = \boldsymbol{A}^{-1}\boldsymbol{E}$, where the matrix $\boldsymbol{E}$ represents the integration over the cells; the matrix $\boldsymbol{A}$ is a mix of the matrices $\boldsymbol{H}$ and $\boldsymbol{G}$ usually defined in the boundary element method. The integral representation for the elastic forces $\dot{N}_{ij}^{e}$ can be obtained from eqn (4), after applying the Hooke's law. After transforming eqn (4) into an algebraic equation, we can write the following algebraic equation of elastic force increments at each cell node:

$$\Delta \boldsymbol{N}^{e(\boldsymbol{BEM})} = \Delta \boldsymbol{K}_N + \boldsymbol{S}_N \Delta \boldsymbol{N}^0, \tag{6}$$

where $\Delta \boldsymbol{K}_N$ is the elastic solution, and $\boldsymbol{S}_N$ defines the corrections due to the dissipative forces $\Delta \boldsymbol{N}^0$.

To define the plate equilibrium equation, we need now to write algebraic equation for the forces $\Delta \boldsymbol{N}^{\boldsymbol{BEM}}$ computed considering the stress field that satisfy the constitutive model (for more details see Fernandes and de Souza Neto [7]):

$$\Delta \boldsymbol{N}^{\boldsymbol{BEM}} = \boldsymbol{C}_N \Delta \boldsymbol{\varepsilon} - \Delta \boldsymbol{K}_N - \boldsymbol{S}_N \Delta \boldsymbol{N}^{\boldsymbol{0}} + \Delta \boldsymbol{N}, \tag{7}$$

where the $\boldsymbol{C}_N$ matrix defines the elastic matrix of all cell nodes; for a node k, $\Delta \boldsymbol{N}^{\boldsymbol{0}(k)}$ is computed considering its total strain $\Delta \boldsymbol{\varepsilon}$ and forces $\Delta \boldsymbol{N}$, i.e., $\Delta \boldsymbol{N}^{\boldsymbol{0}(k)} = \boldsymbol{C}_N^{(k)} \Delta \boldsymbol{\varepsilon}^{(k)} - \Delta \boldsymbol{N}^{(k)}$, where $\Delta \boldsymbol{N}^{(k)}$ satisfies the constitutive model or in our case, it is computed from the homogenised stress vector of the RVE.

Considering a load increment n, the plate equilibrium is achieved, when the following expression is satisfied:

$$\Delta \boldsymbol{K}_{N(n)} - \Delta \boldsymbol{N}^{\boldsymbol{BEM}} = \boldsymbol{0}. \tag{8}$$

Replacing eqn (7) into eqn (8) the plate equilibrium equation can be expressed in terms of total in-plane strains:

$$\boldsymbol{R}_N(\Delta \boldsymbol{\varepsilon}_n) = 2\Delta \boldsymbol{K}_{N(n)} - \boldsymbol{C}_N \Delta \boldsymbol{\varepsilon}_n + \boldsymbol{S}_N(\boldsymbol{C}_N \Delta \boldsymbol{\varepsilon}_n - \Delta \boldsymbol{N}_n) - \Delta \boldsymbol{N}_n = \boldsymbol{0}. \tag{9}$$

When all plate points behave elastically eqn (9) is automatically satisfied. Otherwise an iterative procedure ($i \geq 1$) is required to obtain residual forces ($\boldsymbol{R}_N$) null, where additive corrections $\boldsymbol{\delta \Delta \varepsilon_n^{i+1}}$ must be added to the macro-strain vector ($\boldsymbol{\Delta \varepsilon_n^i}$), i.e., $\boldsymbol{\Delta \varepsilon_n^{i+1}} = \boldsymbol{\Delta \varepsilon_n^i} + \boldsymbol{\delta \Delta \varepsilon_n^{i+1}}$. For that, we apply the Newton–Raphson's scheme to eqn (9). Initially, the strain increment $\boldsymbol{\Delta \varepsilon_n^0}$ is computed from the elastic solution ($\boldsymbol{\Delta K}_N$) for all cell nodes and a RVE is assigned to each one of these nodes. After imposing $\boldsymbol{\Delta \varepsilon_n^0}$ to its respective RVE, we obtain the RVE homogenised response for all cell nodes and eqn (9) is checked. We consider that eqn (9) is satisfied when $\frac{\sqrt{R_N^T R_N}}{\sqrt{\Delta K_N^T \Delta K_N}} \leq tol$, tol being a given tolerance. If it is not satisfied, new corrections ($\boldsymbol{\delta \Delta \varepsilon_n^{i+1}}$) must be obtained and the process continues at iteration i + 1. The corrections $\boldsymbol{\delta \Delta \varepsilon_n^{i+1}}$ are obtained from the linearisation of eqn (9) i.e.,

$$\boldsymbol{\delta\Delta\varepsilon_n^{i+1}} = -\left[\frac{\partial \boldsymbol{R_N}(\boldsymbol{\Delta\varepsilon_n^i})}{\partial \boldsymbol{\Delta\varepsilon_n^i}}\right]^{-1} \boldsymbol{R_N}(\boldsymbol{\Delta\varepsilon_n^i}), \tag{10}$$

where: $-\frac{\partial \boldsymbol{R_N}\left(\boldsymbol{\Delta\varepsilon_n^{(i)}}\right)}{\partial \boldsymbol{\Delta\varepsilon_n^{(i)}}} = \boldsymbol{S_N}\left(\boldsymbol{C_{N(n)}^{ep(i)}} - \boldsymbol{C_N}\right) + \boldsymbol{C_N} + \boldsymbol{C_{N(n)}^{ep(i)}}$ is the consistent tangent operator (CTO), obtained by differentiating eqn (9). The $\boldsymbol{C_{N(n)}^{ep(i)}}$ matrix contains the $\boldsymbol{C_N^{ep}}$ tensor of all cell points. For a node *k*, $\boldsymbol{C_N^{ep(k)}} = \boldsymbol{tC^{ep(k)}}$, where $\boldsymbol{C^{ep(k)}}$ is the inelastic tangent constitutive tensor of the cell node *k* (it is given by the homogenised constitutive tensor of the RVE assigned for node *k*).

3 BEM FORMULATION FOR THE MICROCONTINUUM PROBLEM

In the multi-scale analysis, the constitutive model is defined by the RVE homogenised response. Therefore, one RVE must be assigned for each cell node (*x*) of the macro-continuum (see Fig. 1, where *y* denotes a RVE point and Ω_μ the RVE domain). The RVE has a matrix Ω_1 where we can insert inclusions and/or voids (see Fig. 2). Besides, along the interfaces between matrix and inclusions we can define cohesive-contact finite elements to model the phase debonding that occurs during the fracture process (see Pituba et al. [9]). If these cohesive-contact elements are not defined, the interface is considered perfectly bonded.

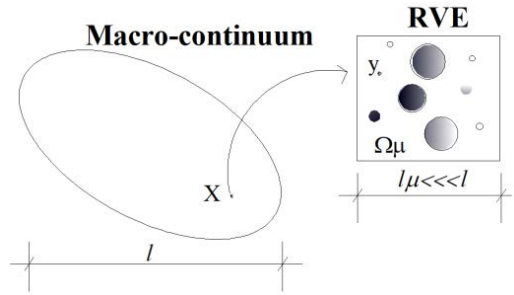

Figure 1: Representation of the macro-continuum and the RVE.

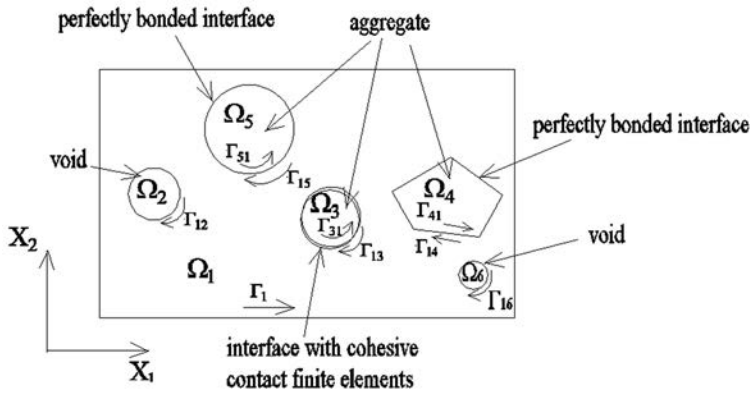

Figure 2: RVE modelling a heterogeneous microstructure where the microcracking process can occur in the ITZ region.

The integral representation of in-plane displacements ($\dot{u}_i^{\mu}$) in the microstructure can be obtained from Bettis's theorem, considering a zoned plate where each sub-region can have different Young's modulus and Poisson's ratio. It is also important to stress that the material behaviour at each RVE phase (matrix and inclusions) can be governed by different constitutive models. The integral representation of in-plane displacements ($\dot{u}_i^{\mu}$) in the RVE is defined as (see Fernandes et al. [5], [6] and Silva et al. [8]):

$$C_{k1}\dot{u}_1^{\mu}(s) + C_{k2}\dot{u}_2^{\mu}(s) = -\frac{\overline{E}_1\nu_1}{\overline{E}\nu}\int_{\Gamma_1}\left(\dot{u}_1^{\mu}(P)p_{k1}^{*(\mu)}(s,P) + \dot{u}_2^{\mu}(P)p_{k2}^{*(\mu)}(s,P)\right)d\Gamma +$$

$$-\sum_{m=1}^{N_{inc}}\frac{(\overline{E}_m\nu_m-\overline{E}_1\nu_1)}{\overline{E}\nu}\int_{\Gamma_{m1}}\left(\dot{u}_1^{\mu}(P)p_{k1}^{*(\mu)}(s,P) + \dot{u}_2^{\mu}(P)p_{k2}^{*(\mu)}(s,P)\right)d\Gamma_{m1}$$

$$-\sum_{m=1}^{N_{voids}}\frac{\overline{E}_1\nu_1}{\overline{E}\nu}\int_{\Gamma_{1m}}\left(\dot{u}_1^{\mu}(P)p_{k1}^{*(\mu)}(s,P) + \dot{u}_2^{\mu}(P)p_{k2}^{*(\mu)}(s,P)\right)d\Gamma_{1m}$$

$$+\int_{\Gamma_1}\left(u_{k1}^{*(\mu)}(s,P)\dot{p}_1^{\mu}(P) + u_{k2}^{*(\mu)}(s,P)\dot{p}_2^{\mu}(P)\right)d\Gamma$$

$$-\overline{E}_1\left(1-\frac{\nu_1}{\nu}\right)\int_{\Gamma_1}\left[\dot{u}_1^{\mu}(P)\varepsilon_{k1}^{*(\mu)}(s,P) + \dot{u}_2^{\mu}(P)\varepsilon_{k2}^{*(\mu)}(s,P)\right]d\Gamma +$$

$$-\sum_{m=1}^{N_{inc}}\left[\overline{E}_m\left(1-\frac{\nu_m}{\nu}\right)-\overline{E}_1\left(1-\frac{\nu_1}{\nu}\right)\right]\int_{\Gamma_{m1}}\left[\dot{u}_1^{\mu}(P)\varepsilon_{k1}^{*(\mu)}(s,P) + \dot{u}_2^{\mu}(P)\varepsilon_{k2}^{*(\mu)}(s,P)\right]d\Gamma_{m1}$$

$$+\sum_{m=1}^{N_S}\overline{E}_m\left(1-\frac{\nu_m}{\nu}\right)\int_{\Omega_m}\dot{u}_i^{\mu}(p)\varepsilon_{kij,j}^{*(\mu)}(s,p)d\Omega_m + \int_{\Omega}\ \varepsilon_{kij}^{*(\mu)}\dot{N}_{ij}^{0(\mu)}\,d\Omega \qquad k,i,j = 1,2, \qquad (11)$$

where the fundamental values (terms with *), ν and $\overline{E}$ are related to the sub-region where the source point s is placed, $\overline{E}_m = \frac{\overline{E}_m}{(1-\nu_m{}^2)}$, $\bar{E}_m = E_m t$; E is Young's modulus, ν the Poisson's ratio, t the plate thickness and δ_{ij} the Kronecker's delta; N_s the sub-regions number; k the fundamental load direction; the subscript '1' refers to the matrix; Γ_1 is the external boundary; Γ_{m1} represents a matrix/inclusion interface; Γ_{1m} is a matrix/void interface. For internal collocation points, $C_{ki} = 1$ and $C_{ki} = 0$, respectively, for $k = i$ and $k \neq i$; for boundary or interface collocation points, the free terms C_{k1} and C_{k2} can be found in the works of Fernandes et al. [4], [5]. All fundamental expressions can be found in Fernandes et al. [4].

In eqn (11), $\dot{N}_{ij}^0$ are dissipative forces, which are defined as:

$$\dot{N}_{ij}^{0(\mu)} = \dot{N}_{ij}^{p(\mu)} - \dot{N}_{ij}^{cf(\mu)}, \qquad (12)$$

where $\dot{N}_{ij}^{p(\mu)}$ is related to the plastic process and $\dot{N}_{ij}^{cf(\mu)}$ to the phase debonding; these forces are defined as:

$$\dot{N}_{ij}^{p(\mu)} = \dot{N}_{ij}^{e(\mu)} - \dot{N}_{ij}^{\mu}, \qquad (13)$$

$$\dot{N}_{ij}^{cf(\mu)} = \dot{N}_{ij}^{e(\mu)} - \dot{\bar{N}}_{ij}^{\mu}. \qquad (14)$$

In eqn (14) the continuous forces $\dot{\bar{N}}_{ij}^{\mu}$ are given by the elastic forces computed before solving the RVE equilibrium problem (see Fernandes et al. [5]). Note that after achieving the RVE equilibrium, the strain field becomes discontinuous if the phase debonding occurred on

interfaces. In eqn (13) the forces $\dot{N}_{ij}^{\mu}$ satisfy the constitutive model adopted to govern mechanical behaviour in the RVE phase, while the elastic membrane forces $\dot{N}_{ij}^{e(\mu)}$ are computed from the total strain, i.e.,

$$\dot{N}_{ij}^{e(\mu)} = \frac{\overline{E}}{(1-\nu^2)}\left[\nu\,\dot{\varepsilon}_{kk}^{\mu}\delta_{ij} + (1-\nu)\dot{\varepsilon}_{ij}^{\mu}\right]. \tag{15}$$

To compute the unknown's problem, we must transform eqn (11) into its algebraic form by considering linear elements on the boundary and interfaces and triangular cells in the domain. In the elements the displacements and tractions vary linearly while in the cells the displacements are approximated by linear functions and the dissipative forces are adopted constant. In the RVE there are two unknowns at boundary nodes (displacements or tractions, according to boundary conditions) and two unknowns at interface and cell nodes (displacements). Thus, to obtain the set of equations necessary to solve the problem, we write two displacement equations at boundary, interface, and cell nodes, resulting into:

$$\begin{bmatrix}[H]_{BB} & [H]_{Bi}\\ [H]_{iB} & [H]_{ii}\end{bmatrix}_{RVE}\begin{Bmatrix}\{\Delta U\}_B\\ \{\Delta U\}_i\end{Bmatrix}_{RVE} = \begin{bmatrix}[G]_{BB}\\ [G]_{iB}\end{bmatrix}_{RVE}\{\Delta P_B\}_{RVE} + \begin{bmatrix}[E]_{BB}\\ [E]_{iB}\end{bmatrix}_{RVE}\{\Delta N^0\}_{RVE}, \tag{16}$$

where $\boldsymbol{U}$ and $\boldsymbol{P}$ refer, respectively to nodal displacements and tractions, subscript *B* refers to the boundary, subscript *i* refers to interface or internal node; in a simplified form eqn (16) is defined as:

$$[H]_{RVE}\{\Delta U\}_{RVE} = [G]_{RVE}\{\Delta P_B\}_{RVE} + [E]_{RVE}\{\Delta N^0\}_{RVE}. \tag{17}$$

In the RVE the boundary conditions are defined by the imposition of the strain vector of the macro-continuum point, i.e., a constant strain is imposed to the RVE what implies to impose linear displacements to the boundary nodes. After imposing these boundary conditions to eqn (17), the unknown values (ΔX_{RVE}) can be computed (see Fernandes et al. [4]):

$$\{\Delta X\}_{RVE} = \{\Delta L\}_{RVE} + [R]_{RVE}\{\Delta N^0\}_{RVE}, \tag{18}$$

where $\{\Delta X\}_{RVE} = \begin{Bmatrix}\{\Delta P\}_B\\ \{\Delta U\}_i\end{Bmatrix}_{RVE}$, $\{\Delta L\}_{RVE}$ represents the elastic solution; $\{\Delta L\}_{RVE} = [A]_{RVE}^{-1}\{\Delta B\}_{RVE}$; $[R]_{RVE} = [A]_{RVE}^{-1}[E]_{RVE}$; $\{\Delta B\}_{RVE} = \begin{bmatrix}-[H]_{BB}\\ -[H]_{iB}\end{bmatrix}_{RVE}\{\Delta U_B\}_{RVE}$; $[A]_{RVE} = \begin{bmatrix}-[G]_{BB} & [H]_{Bi}\\ -[G]_{iB} & [H]_{ii}\end{bmatrix}_{RVE}$.

Solving the problem, however, requires the algebraic equation of the membrane forces, $\{\Delta\bar{N}\}_{RVE}^{BEM}$ at the centre of each cell, defined by:

$$\{\Delta\bar{N}\}^{BEM} = -[[H']_B \quad [H']_i]_{RVE}\begin{Bmatrix}\{\Delta U\}_B\\ \{\Delta U\}_i\end{Bmatrix}_{RVE} + [G_B']_{RVE}\{\Delta P_B\}_{RVE} + [E']_{RVE}\{\Delta N^0\}_{RVE}. \tag{19}$$

To solve eqn (19) we have to impose linear displacements to the boundary nodes, resulting in:

$$\{\Delta\bar{N}\}_{RVE}^{BEM} = \{\Delta K\}_{RVE} + [S]_{RVE}\{\Delta N^0\}_{RVE}. \tag{20}$$

where$\{\Delta K\}_{RVE} = \{\Delta B'\}_{RVE} - [A']_{RVE}\{\Delta L\}_{RVE}$;$[S]_{RVE} = [E']_{RVE} - [A']_{RVE}[R]_{RVE}$; $\{\Delta B'\}_{RVE} = -[H'_B]_{RVE}\{\Delta U_B\}_{RVE}$; $[A']_{RVE} = [-[G'_B]_{RVE} \quad [H'_i]_{RVE}]$.

On the other hand, the RVE displacement field, $\boldsymbol{u_\mu(y)}$, contains the displacement field due to the imposed macroscopic strain ($\boldsymbol{u_\mu^\varepsilon(y)}$) and the displacement fluctuation field ($\boldsymbol{\tilde{u}_\mu(y)}$), i.e.,

$$\boldsymbol{u_\mu(y) = u_\mu^\varepsilon(y) + \tilde{u}_\mu(y)}. \tag{21}$$

Accordingly, the microscopic strain field can also be decomposed into the macroscopic strain $\boldsymbol{\varepsilon(x) = \varepsilon}$ and the strain fluctuation field $\boldsymbol{\tilde{\varepsilon}_\mu}$ ($\boldsymbol{\tilde{\varepsilon}_\mu = B\tilde{u}_\mu}$), where $\boldsymbol{B}$ is the strain-displacement matrix of the finite element method).

In turn, the RVE equilibrium problem is achieved when the stress field is self-equilibrated. For that, the following equilibrium equation must be satisfied:

$$R_F = \sum_{e=1}^{N_{cell}^\mu} B_e^T \Delta\sigma_\mu^{e(i)} t\, A_e = \sum_{e=1}^{N_{cell}^\mu} [B]_e^T t\left[D_\mu^e\right]\left(\{\Delta\varepsilon\} + [B]\{\Delta\tilde{u}_\mu\}\right)_e A_e = 0, \tag{22}$$

where subscript *e* refers to a cell; N_{cell}^μ is the cell number in the RVE domain; *t* is the macro-continuum thickness; $\left[D_\mu^e\right]$ is the constitutive tensor, B_e the strain-displacement matrix; A_e the cell area.

If eqn (22) is not verified an iterative procedure $i_{RVE} \geq 0$ is required where corrections $\delta\tilde{u}_\mu^{i_{RVE}+1}$ must be added to the fluctuation increment at iteration $i_{RVE}+1$, i.e., $\Delta\tilde{u}_\mu^{i_{RVE}+1} = \Delta\tilde{u}_\mu^{i_{RVE}} + \delta\tilde{u}_\mu^{i_{RVE}+1}$. These corrections are computed from the following expression:

$$\boldsymbol{\Delta F^{i_{RVE}} + K^{i_{RVE}}\delta\tilde{u}_\mu^{i_{RVE}+1} = 0}, \tag{23}$$

where the matrix *K* is the CTO operator and F the nodal forces vector given by:

$$\boldsymbol{K^{i_{RVE}} = \sum_{e=1}^{N_{cel}} B_e^T D_\mu^{(e)i_{RVE}} B_e t\, A_e + \sum_{ef=1}^{N_f} K_{ef}^{i_{RVE}} t}, \tag{24}$$

$$\boldsymbol{\Delta F^{i_{RVE}} = \sum_{e=1}^{N_{cel}} B_e^T \Delta\sigma_\mu^{e(i_{RVE})} t\, A_e + \sum_{ef=1}^{N_f} \Delta F_{ef}^{i_{RVE}} t}, \tag{25}$$

being N_f the number of cohesive contact fracture element; subscript *e* and *ef* refers, respectively to the triangular cell and cohesive contact element.

These cohesive contact finite elements are rectangular; they have four nodes and are placed on the interfaces between inclusions and matrix to model the phase debonding (see Fig. 3). Their nodes are adopted coincident to the interface and cell nodes (see Fig. 3). For more details about the definition of $\boldsymbol{K_{ef}}$ and $\boldsymbol{F_{ef}}$, please see Pituba et al. [9].

The RVE homogenised constitutive tensor is defined as:

$$\boldsymbol{C^{ep} = C^{ep(Taylor)} + \tilde{C}^{ep}}, \tag{26}$$

where $\boldsymbol{C^{ep(Taylor)} = \sum_{p=1}^{N_p} \frac{V_p}{V_\mu} D_\mu^{(p)}}$;$\boldsymbol{\tilde{C}^{ep} = -\frac{1}{V_\mu} G_R K_R{}^{-1} G_R{}^T}$; N_p is the number of phases of the RVE; V_μ is the RVE volume; $\boldsymbol{G = \sum_{e=1}^{N_{cell}^{RVE}} D_\mu^e B_e V_e}$.

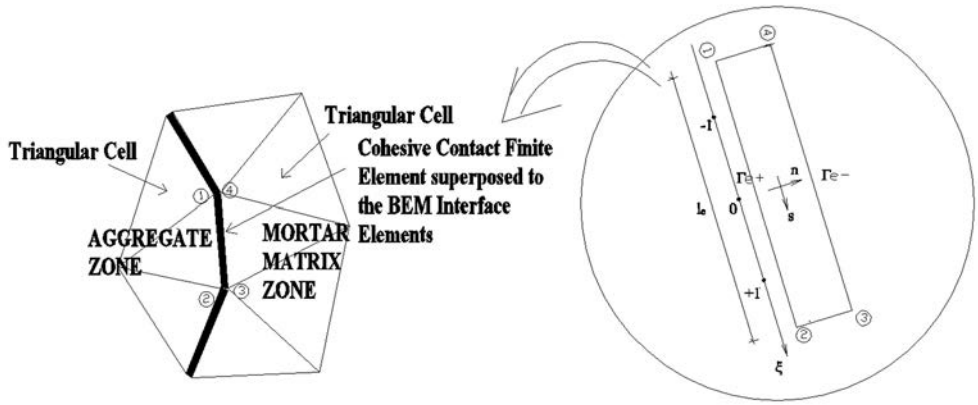

Figure 3: Cohesive contact finite element and its insertion between triangular cells.

The $C^{ep(Taylor)}$ tensor is obtained by assuming the displacement fluctuation field null while $\tilde{C}^{ep}$ represents the influence of the displacement fluctuation. The RVE homogenised stress tensor is defined as:

$$\boldsymbol{\sigma} = (\bar{\boldsymbol{\sigma}} + \bar{\boldsymbol{\sigma}}^{\boldsymbol{T}})\frac{1}{2V_{\mu}}, \tag{27}$$

where $\bar{\sigma} = \sum_{i=1}^{N_b}\{F\}_i\{y\}_i^T$, N_b being the number of nodes on the external boundary, $\boldsymbol{F}$ the forces at these boundary nodes and $\boldsymbol{y}$ their coordinates vector. The forces $\boldsymbol{F}$ are defined as:$\{F_i\}_n = \{P_B\}_n\frac{1}{2}(L_{e-1} + L_e)$, where $\{P_B\}_n = \{P_B\}_{n-1} + \{\Delta P_B\}_n$, L is the element length, n is the increment of the macro-continuum problem; $\{\Delta P_B\}_n$ is obtained from eqn (16).

Note that when the RVE equilibrium is achieved, we must add the displacement increment fluctuation field to the nodal boundary displacements $\{\Delta U_B\}_n$. Then, we must update the boundary tractions $\{\Delta P_B\}_n$ by using eqn (16).

4 NUMERICAL EXAMPLE

Consider the plate depicted in Fig. 4(a), subjected to compression force. Its discretisation is depicted in Fig. 4(b), where only one quarter of the plate is defined, for symmetry reasons. The plate thickness is 1mm and it is discretised by 16 boundary elements and 16 cells. We define two elements at each smaller side and six elements along each bigger side. The plate boundary conditions are defined as: tractions $p_s = 0$ $p_n = -25$ N/mm to the nodes 19 to 23; tractions $p_s = p_n = 0$ to nodes 6 to 18; $u_n = 0$ and p_s=0 to the nodes 1 to 5 and to the nodes 24 to 36.

The concrete microstructure is modelled considering two RVEs (see Fig. 5). RVE-25i is composed of 25 aggregates of different dimensions (see Table 1) and 12 voids of 6 mm diameter, randomly distributed in the mortar domain; RVE-5i is defined by five aggregates (four of 33 mm diameter and one of 27 mm diameter) and four voids of 10.4 mm diameter, symmetrically distributed in the domain. The volume fractions of inclusions and voids remains the same, being defined, respectively, as 40% and 3.39%. Their discretisation is defined in Table 2.

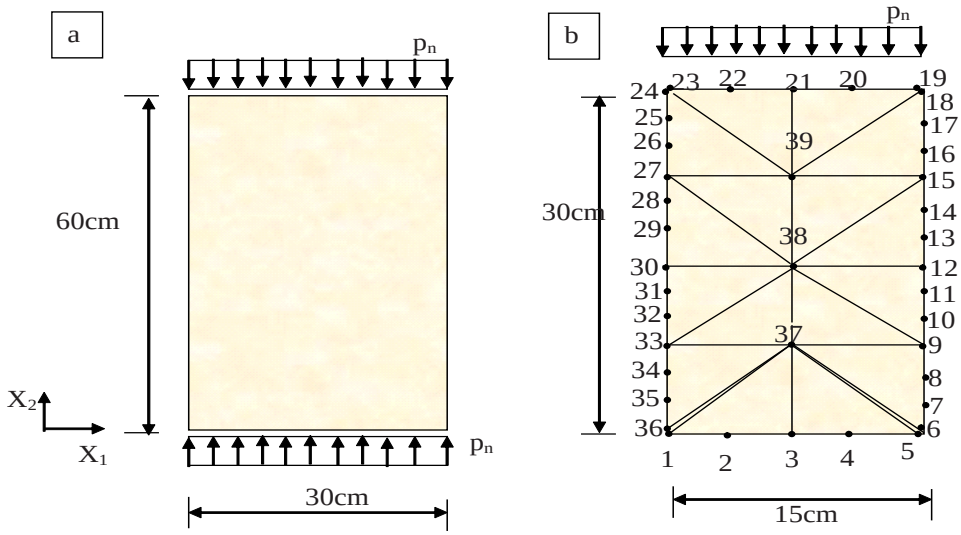

Figure 4: (a) Geometry and loads of the plate; and (b) Discretisation of the plate.

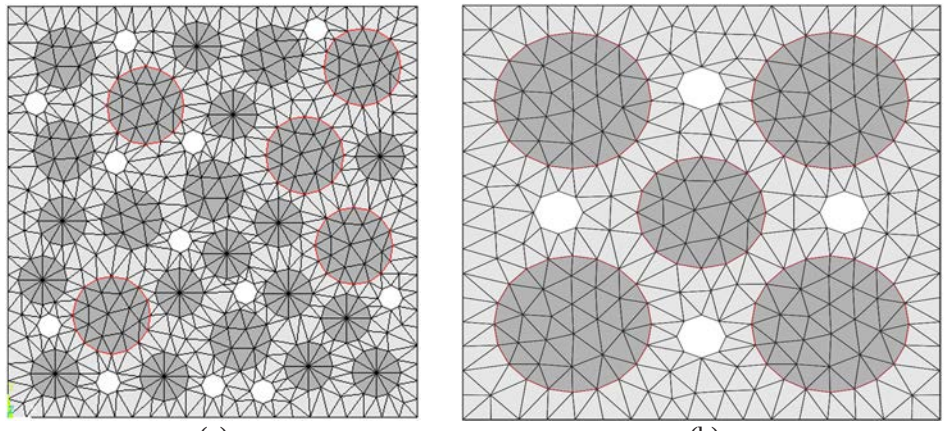

Figure 5: Microstructure and discretisation of the RVEs. (a) RVE-25i; and (b) RVE-5i.

Table 1: Quantity and dimensions of aggregates for each RVE.

RVE	**Total number of aggregates**	**Aggregate diameter/aggregate quantity**			**Aggregates volume fraction**
RVE-5i	5	33 m	27 mm		40.00%
		4	1		
RVE-25i	25	19 mm	15 mm	12 mm	40.61%
		5	6	14	

Table 2: Discretisation of RVES.

RVE	Discretisation					
	No. of nodes	No. of cells	No. of boundary elements	No. of inclusion interface nodes	No. of void interface nodes	No. of cohesive-contact elements
RVE-5i	403	520	68	192	32	96
RVE-25i	721	1116	129	496	96	80

The aggregates are considered elastics with Young's modulus (E) = 40 GPa and Poisson's ratio (v) = 0.3, while the mortar matrix is governed by Mohr–Coulomb criterion, with friction angle equal to 4°, E = 23 GPa, v = 0.2. The plastic curve of the Mohr–Coulomb $((\bar{\varepsilon}_{p,}\sigma_y))$ where $\bar{\varepsilon}_p$ is the effective plastic strain and σ_y the yield stress, is adopted, respectively, for RVE-25i and RVE-5i (0; 11.0) and (0.22; 70); (0; 11.7) and (0.22; 46). For RVE-25i the cohesive contact finite elements are defined only around the bigger aggregates, whereas for RVE-5i they are defined around all aggregates. Their parameters are defined as: β_c = 0.707; σ_c = 2 MPa; δc = 0.0568 mm; λ_p = 200,000. The value β_c is related to the sliding and normal opening displacements (the higher its value, the greater sliding displacement importance); σ_c is the maximum cohesive normal traction; δc is a characteristic opening displacement; the penalty factor λ_p is used in the contact model and it is related to the stiffness between triangular cells.

Fig. 6 shows the displacement u_n at node 21 (see Fig. 4) throughout the load incremental process, comparing the results to the model where the finite element formulation discussed in Pituba et al. [9] models the RVE. 'Plate 1' is the plate where RVE-5i is used while RVE-25i is considered in 'Plate 2'. Fig. 7 compares the experimental curve to the numerical results.

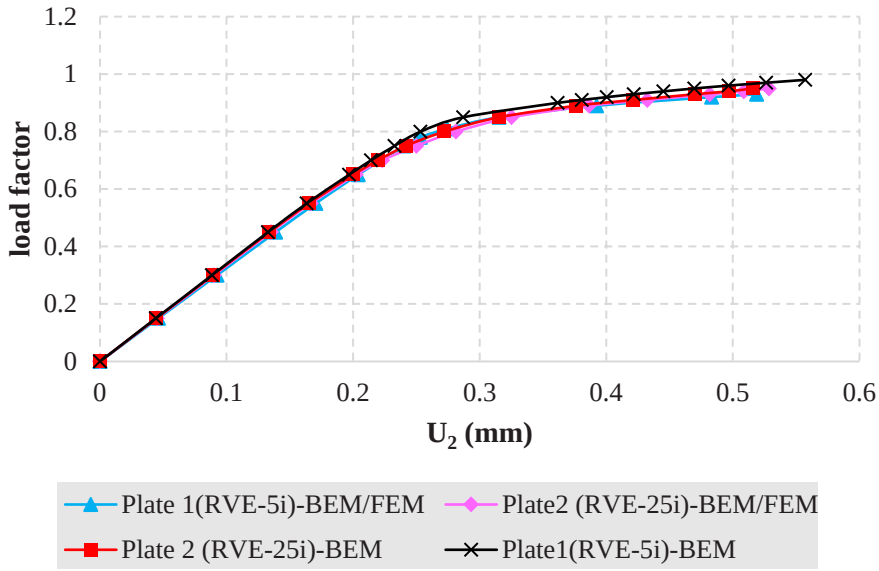

Figure 6: Displacement at the plate point 21 throughout the load incremental.

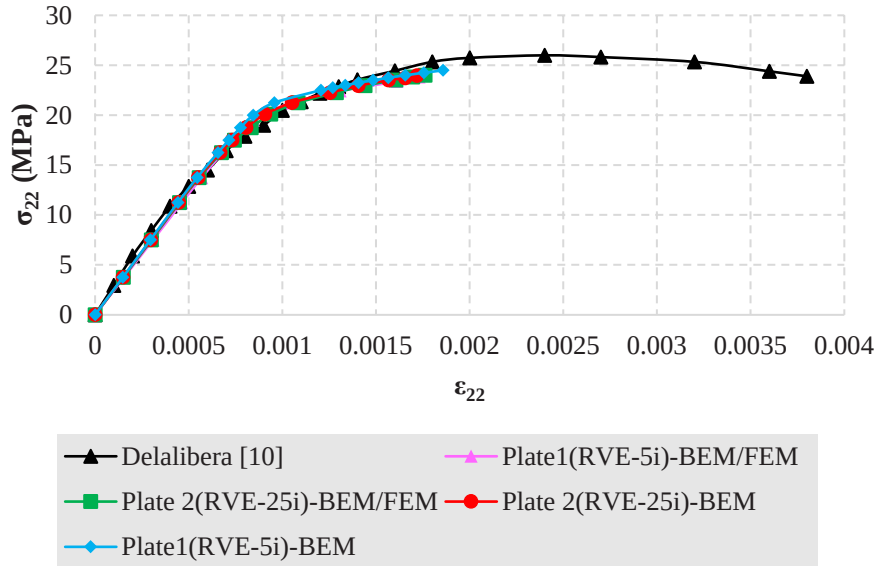

Figure 7: Stress versus strain in x_2 direction, comparing the numerical results to the experimental ones given in Delalibera [10].

We can observe that the plates present similar mechanical behaviour what means that a simple RVE can reproduce good results when only compression loads are considered. But it is important to stress that for more complex types of loading the RVEs will not present similar results, as the fracture process plays an important role when tension or shear stresses are considered. Besides, we observe that the BEM/FEM model presents similar results to the model where only BEM is considered. But the BEM model has reduced computational effort (see Table 3, where t_{BEM} refers to the computational time of BEM model and $t_{BEM/FEM}$ to the computational time of BEM/FEM model). Table 3 also shows, as expected, that the computational time $t_{(plate\ 2)}$ related to 'Plate 2' is much bigger than the time related to 'Plate 1' $t_{(plate\ 1)}$.

Table 3: Comparison of the computational effort.

Plate 1 (RVE-5i) $t_{BEM}/t_{BEM/FEM}$	**Plate 2 (RVE-25i)** $t_{BEM}/t_{BEM/FEM}$	**BEM** $t_{plate\ 1}/t_{plate\ 2}$	**BEM/FEM** $t_{plate\ 1}/t_{plate\ 2}$
0.566	0.5665	0.1787	0.1789

Fig. 7 shows that the numerical results compare well to the experimental test, showing that the model is robust and efficient.

ACKNOWLEDGEMENTS

The authors want to thank CNPq (National Council for Scientific and Technological Development) (grant numbers 302809/2020-1) and FAPEG (Goiás Research Foundation) (grant number 202410267000680) for the financial support.

REFERENCES

[1] Peric, D., de Souza Neto, E.A., Feijóo, R., Partovi, M. & Molina, A.C., On micro-to-macro transitions for multiscale analysis of heterogeneous materials: Unified variational basis and finite element implementation. *Int. J. Numer. Methods Engrg.*, **87**, pp. 149–170, 2011.

[2] Somer, D.D., de Souza Neto, E.A., Dettmer, W.G. & Peric, D., A sub-stepping scheme for multi-scale analysis of solids. *Comput. Methods Appl. Mech. Engrg*., **198**, pp. 1006–1016, 2009.

[3] Fernandes, G.R., Pituba, J.J.C. & de Souza Neto, E.A., FEM/BEM formulation for multi-scale analysis of stretched plates. *Eng. Anal. Bound. Elem.*, **54**, pp. 47–59, 2015.

[4] Fernandes, G.R., Crozariol, L.H.R., Furtado, A.S. & Santos, M.C., A 2D boundary element formulation to model the constitutive behaviour of heterogeneous microstructures considering dissipative phenomena. *Eng. Anal. Bound. Elem*., **99**, pp. 1–22, 2019. https://doi.org/10.1016/j.enganabound.2018.10.018.

[5] Fernandes, G.R., Marques, M.J., Vieira, J.F. & Pituba, J.J.C., A RVE formulation by the boundary element method considering phase debonding. *Eng. Anal. Bound. Elem*., **104**, pp. 259–276, 2019. https://doi.org/10.1016/j.enganabound.2019.03.018.

[6] Fernandes, G.R., Pontes, G.B.S., Oliveira, V.N., A 2D BEM formulation considering dissipative phenomena and a full coupled multiscale modelling. *Eng. Anal. Bound. Elem*., **119**, pp. 25–43, 2020. https://doi.org/10.1016/j.enganabound.2020.07.004.

[7] Fernandes, G.R. & de Souza Neto, E.A., Self-consistent linearization of non-linear BEM formulations with quadratic convergence. *Computational Mechanics*, **52**, pp. 1125–1139, 2013.

[8] Silva, M.J.M., Pitaluga, C.G., Fernandes, G.R. & Pituba, J.J.C., Meso-scale modeling of the compressive mechanical behavior of concrete by a RVE-based BEM formulation. *Mechanics of Advanced Materials and Structures*, **1**, pp. 1–20, 2022.

[9] Pituba, J.J.C., Fernandes, G.R. & Souza Neto, E.A., Modeling of cohesive fracture and plasticity processes in composite microstructures. *Journal of Engineering Mechanics*, **142**, 04016069, 2016. https://doi.org/10.1061/(ASCE)EM.1943-7889.0001123.

[10] Delalibera, R.G., Theorical and experimental analysis of reinforced concrete beams with confinement reinforcement. Master's thesis, University of Sao Paulo, São Paulo, Brazil, 2002. (In Portuguese.)